PROCEEDINGS A

royalsocietypublishing.org/journal/rspa

Research

Check for updates

Article submitted to journal

Subject Areas:
Mechanical engineering, Mechanics, Computational mechanics

Keywords:
Nonlinear vibrations, Secondary resonance, Two-harmonic forcing, Simultaneous resonance, Isola, Homotopy

Author for correspondence:
G. Raze
e-mail: g.raze@uliege.be

A two-harmonic homotopy method to connect a primary resonance to its secondary resonances

G. Raze and G. Kerschen

Space Structures and Systems Laboratory, Aerospace and Mechanical Engineering Department, University of Liège
Quartier Polytech 1 (B52/3), Allée de la Découverte 9, B-4000 Liège, Belgium

Besides the well-known primary resonances, forced nonlinear systems can exhibit secondary (namely superharmonic, subharmonic and ultrasubharmonic) resonances whose frequencies are rationally related to the forcing frequency. Some of these secondary resonances can appear as isolated branches of solutions, challenging their characterization. This work leverages two-harmonic forcing to transition from a primary resonance to a specific secondary resonance. A homotopy problem is formulated, whose limit cases correspond to these resonances. The proposed method is shown to be able to uncover isolated responses in a deterministic and reliable way. It is illustrated on a Duffing oscillator, a two-degree-of-freedom system and a beam with contact.

1. Introduction

The concept of resonance is central in vibration engineering and nonlinear dynamics. Akin to their linear counterparts, primary resonances are arguably one of the most important features of a nonlinear system since they are associated with high-amplitude responses. Secondary resonances however have received much less attention, but can be a threat [1,2] or an opportunity [3–7] depending on the application at hand. These resonances are usually identified with two incommensurate natural numbers, m and l. For an m:l resonance, the period of motion is l times greater than the forcing period, and the m^{th} harmonic of this motion is generally prominent. One challenge associated with these resonances is that some of them can be isolated [8,9], making them difficult to reach with traditional methods.

THE ROYAL SOCIETY PUBLISHING

There exist numerical methods for global analysis [10–13] that find isolated solutions, but they are generally expensive, especially for large-scale systems. Cheaper alternatives were proposed in [14–17]. Salles et al [14] proposed a strategy to compute isolas near imperfect bifurcations. In Ponsioen et al [15], nonlinear model order reduction techniques are used, but these are limited to relatively weak forcing amplitudes. Vadcard et al [16] relied on an energy balance principle which is computationally inexpensive but theoretically limited to primary and subharmonic resonances [18]. Finally, Quaegebeur et al [17] very recently proposed an alternative continuation approach capturing a wide variety of isolas. We also note that bifurcation tracking procedures can be used to follow isolated responses [19–21] provided an initial point on the isola is available. Such a point can generally only be found for the class of isolas that merge with the main response. This approach can also be used as a basis for optimization procedures [22,23].

The vast majority of studies of periodically-forced nonlinear systems deal with single-harmonic (or tonal) forcing. Multi-harmonic forcing can naturally appear in the problem under study, e.g., in rotating machinery [24]. It can also inadvertently be present in some cases. For instance, in experiments, shaker-structure interactions can result in the presence of significant non-fundamental harmonics, distorting the force applied to the structure [25–27]. Two-harmonic forcing can be used on purpose for multiple reasons. Early studies showed that it could suppress chaos [28], affect the stability of some attractors [29] or influence period-doubling bifurcations [30, 31]. Multi-harmonic, multi-point forcing can also be needed in the field of nonlinear modal testing when one wants to perform modal appropriation of a nonlinear normal mode [32]. The influence of two-harmonic forcing on resonances was studied theoretically, resulting in what is sometimes called a *simultaneous resonance* [33,34]. Parametric studies showed that the basins of attraction of these resonances could be greatly influenced and that they could be suppressed when adapting the parameters of the forcing [35,36]. It is also possible to greatly influence the shape of the nonlinear frequency response through the allocation of different powers to the harmonics [37].

In this work, two-harmonic forcing is leveraged as a proxy to attain any secondary resonance associated to a given mode, wherein a two-term harmonic forcing is considered. Performing a homotopy from the forcing of one harmonic to the other, the resonance is smoothly continued. At the end of the transition, the forcing becomes harmonic again, and the system vibrates according to a secondary resonance, possibly isolated from the main frequency response. This simple and fast method thus provides a numerically tractable way to attain isolated responses.

The rationale behind the method is introduced with a Duffing oscillator in Section 2. The mathematical framework is then outlined in Section 3 and an efficient numerical treatment with the harmonic balance method is developed in Section 4. The method is tested on a Duffing oscillator, a two-degree-of-freedom system and a finite element model of a beam with clearance contact in Sections 5, 6 and 7, respectively, before concluding this work in Section 8.

2. Resonances and two-harmonic forcing

(a) Resonances of a Duffing oscillator

A simple, classical example is considered first to introduce the problem treated in this work, namely the Duffing oscillator. In dimensionless form, this oscillator is governed by

$$\ddot{x}(t) + 2\zeta_0\dot{x}(t) + x(t) + x^3(t) = f(t), \tag{2.1}$$

where x is the displacement of the oscillator, f is the external forcing, ζ_0 is the damping ratio, and an overdot denotes differentiation with respect to the dimensionless time t [38]. In the sequel, $\zeta_0 = 0.025$ is considered unless otherwise stated.

Figure 1 represents the nonlinear frequency response (NFR) of the oscillator described by Equation (2.1) for a harmonic forcing of amplitude 3. This NFR was calculated using a harmonic balance (HB) formalism coupled with a continuation procedure [19,39]. The most prominent feature of this NFR is the 1:1 primary resonance appearing as a bent, large-amplitude peak,

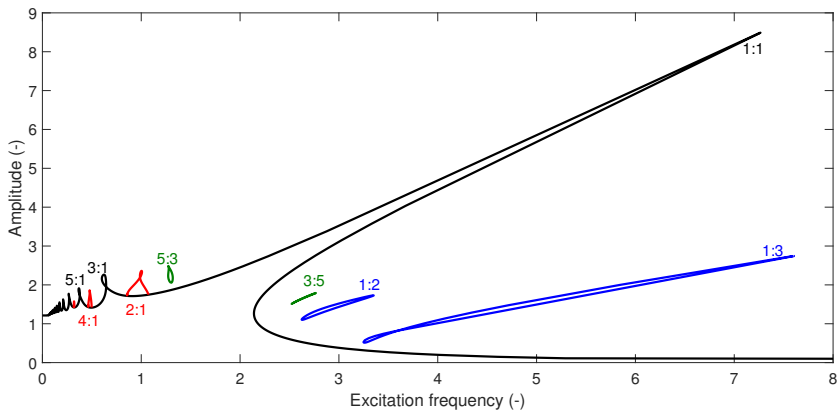

Figure 1: NFR of the Duffing oscillator $\ddot{x}(t) + 0.05\dot{x}(t) + x(t) + x^3(t) = 3\sin(\omega t)$: main branch of the NFR (—), even superharmonic resonances (—), subharmonic resonances (—) and ultrasubharmonic resonances (—).

but other peaks are also observable in the response. Specifically, odd superharmonic resonances (m:1) appear on the main branch at low excitation frequencies. Even superharmonic resonances bifurcate from this branch (through symmetry-breaking bifurcations). In addition, subharmonic (1:l) and ultrasubharmonic (m:l, $m > 1$, $l > 1$, $\gcd(m, l) = 1$, where gcd is the greatest common divisor) resonances manifest themselves as isolas. A larger number of higher-order secondary resonances can appear at higher forcing levels [8,9].

These isolated resonances are challenging to obtain with conventional continuation approaches and require adequate initial conditions [9], typically found with stochastic procedures [40]. These procedures aim to find an initial condition that lies in the basin of attraction of a specific resonance by randomly sampling the space of initial conditions $(x(0), \dot{x}(0))$. Figure 2 depicts such basins of attraction at $\omega = 2.7$ (where the 3:5 and 1:2 resonances coexist with the 1:1 resonance) and $\omega = 6$ (where the 1:3 and 1:1 resonances coexist).

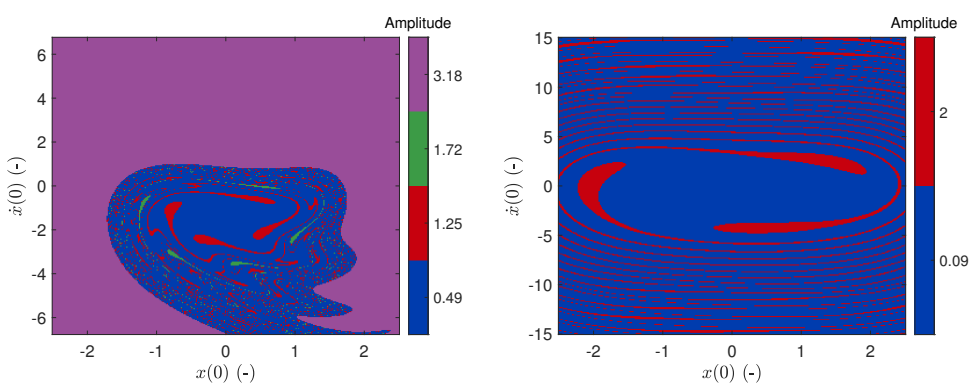

(a) (b)

Figure 2: Basins of attraction of the Duffing oscillator $\ddot{x}(t) + 0.05\dot{x}(t) + x(t) + x^3(t) = 3\sin(\omega t)$ in the set of initial conditions $(x(0), \dot{x}(0)) \in [-2.5, 2.5] \times [-2.5\omega, 2.5\omega]$: $\omega = 2.7$ (a) and $\omega = 6$ (b).

Computing full basins of attraction with an accurate resolution is a time-consuming process, but a random sampling of the initial condition can incur significant savings since a substantially smaller number of time integrations may be required to reach a secondary resonance. To have an idea of how long this procedure can take, the expected time for a random sampling of the initial conditions to reach a given resonance can be estimated as

$$t_{\text{avg}} = \frac{t_0}{p}, \tag{2.2}$$

where t_0 is the CPU time taken by one time integration, and p is the probability to obtain initial conditions that lie within the basin of attraction of the sought resonance. These probabilities were estimated equal to the volume fraction of each basin. t_0 was estimated based on a Runge-Kutta numerical integration procedure (`ode45`) over 500 periods of excitation, which was verified to be enough to reach a steady-state response. Table 1 gathers the expected estimated times. We nevertheless note that they represent an optimistic lower bound for random sampling methods, since educated choices were made for the excitation frequency and range of initial conditions to find the resonances.

Resonance	ω	p	t_{avg} (s)
5:3	1.3	0.7270	0.26
3:5	2.7	0.0081	23.42
1:2	2.7	0.0474	4.01
1:3	6	0.1544	0.33

Table 1: Expected time to find isolated resonances in the set of initial conditions $(x(0), \dot{x}(0)) \in [-2.5, 2.5] \times [-2.5\omega, 2.5\omega]$ with a random sampling procedure.

(b) Two-harmonic forcing

The motivating idea behind the method proposed in this work is now illustrated by considering a two-harmonic forcing as

$$f(t) = 3(\alpha \sin(\omega t) + (1-\alpha)\sin(3\omega t)), \tag{2.3}$$

in Equation (2.1), where α is a factor determining the relative amplitude of the harmonics in the forcing and ω is the fundamental angular frequency of excitation. Most works typically consider single-harmonic forcing, corresponding either to $\alpha = 0$ or $\alpha = 1$. For a fixed value of α, NFRs can once again be obtained with classical continuation approaches. Figure 3a depicts such an NFR for $\alpha = 0$ (to avoid overcrowding the figure, isolas are not depicted). It should be underlined that the frequency axis represents ω and thus does not correspond the excitation frequency in this case. For $\alpha = 1$, the exact same NFR curve is obtained by stretching the frequency axis by a factor 3 (and in this case, it corresponds to the excitation frequency).

A question then arises: what happens to the primary resonance if one progressively increases (or decreases) α from 0 to 1 (or 1 to 0)? Such a situation can be seen as a homotopy problem. Figure 3b depicts such scenarii, wherein the resonance is tracked to help visualizing its evolution (the mathematical framework used herein will be formalized in the next section). Increasing α from 0, the primary resonance gradually shrinks in amplitude and transits as a simultaneous primary and superharmonic resonance, to finally become the 3:1 superharmonic resonance at $\alpha = 1$. Conversely, the primary resonance at $\alpha = 1$ also shrinks as α decreases, albeit more slowly, transits as a simultaneous primary and subharmonic resonance, and eventually becomes the 1:3 subharmonic resonance at $\alpha = 0$. Interestingly, the two-harmonic forcing offers a continuous path toward this 1:3 subharmonic resonance, which is isolated from the main branch of the NFR when one considers a single-harmonic forcing.

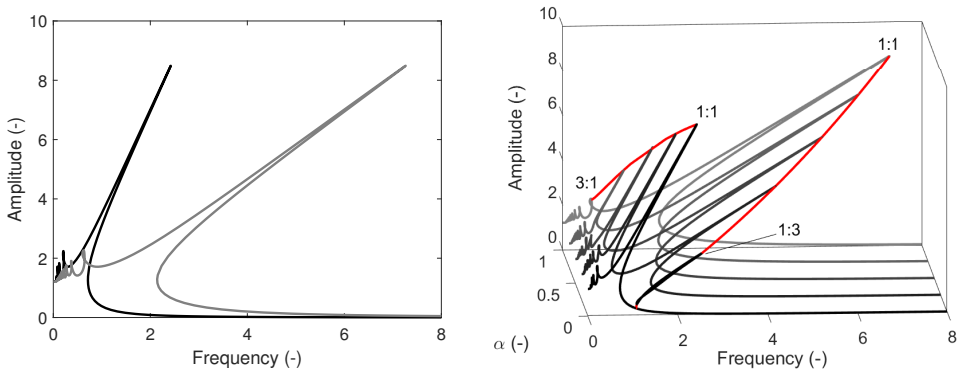

Figure 3: NFRs of the Duffing oscillator under harmonic forcing for $\alpha = 0$ (—) and $\alpha = 1$ (—) (a), and set of NFRs for different values of α (in different levels of gray) with resonance locus (—) (b).

These results suggest that a homotopy between two different single-harmonic forcing cases allows us to reach isolated arbitrary resonances by leveraging two-harmonic forcing. In particular, since the primary resonance of a system is typically easy to detect and reach, one could attain a more challenging and potentially isolated m:l resonance with this simple deterministic method, as depicted in Figure 4 (where f_m and f_l represent the amplitudes of the different forcing harmonics). This idea is developed more formally in the next section, where the method is formulated.

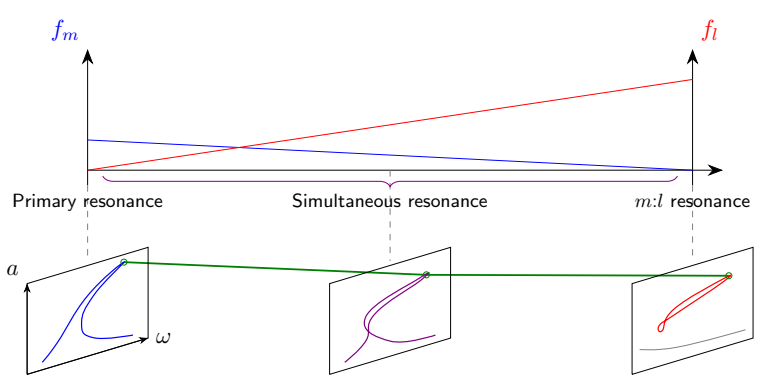

Figure 4: Schematics of the two-harmonic homotopy method. The THHM locus is indicated by — and the points at which it crosses the NFRs (which are defined for constant f_m and f_l) by ○.

3. Two-harmonic homotopy method: formulation

Motivated by the results obtained with the Duffing oscillator, the two-harmonic homotopy method (THHM) is now introduced in a general setting. Figure 4 summarizes the main idea of the proposed THHM. Starting from a point on a given primary resonance at a given $f_m \neq 0$ and $f_l = 0$, one progressively decreases f_m while adjusting f_l (or increases f_l while adjusting f_m). This process continues until $f_m = 0$, in which case an m:l resonance is reached, or a trivial response on

the main frequency branch. The way in which these forcing amplitudes are adapted is governed by user-selected constraints which affect the (possibly) reached $m:l$ resonance.

When one targets a subharmonic or ultrasubharmonic resonance, the mere presence of subharmonic components in the response at the end of the THHM, i.e. when the state $f_m = 0$ is reached, indicates that the sought resonance has been reached. For superharmonic resonances, one should see a prevalence of the m^{th} harmonic in the response. If these cases are not verified, the method likely ended up on the main branch of the NFR and can be considered to be unsuccessful. An analysis of the THHM locus can be useful to gain further insight into the dynamics, as shall be shown in the examples.

The method is now formalized. A system described by a vector of degrees of freedom $\mathbf{x}$ of length N_x and governed by the equations of motion

$$\mathbf{M}\ddot{\mathbf{x}}(t) + \mathbf{C}\dot{\mathbf{x}}(t) + \mathbf{K}\mathbf{x}(t) + \mathbf{f}_{\text{nl}}(\mathbf{x}(t), \dot{\mathbf{x}}(t)) = \mathbf{f}(f_m \sin(m\omega t) + f_l \sin(l\omega t + \phi_l)) \tag{3.1}$$

is considered, where $\mathbf{M}$, $\mathbf{C}$ and $\mathbf{K}$ are linear structural mass, damping and stiffness matrices, respectively, $\mathbf{f}_{\text{nl}}$ is the vector of nonlinear forces, $\mathbf{f}$ is the spatial distribution of external forces and is modulated by two harmonics with amplitudes f_m and f_l and phase ϕ_l.

In the THHM, parameters ω, f_m, f_l are variable, whereas ϕ_l is fixed to a user-defined value depending on the targeted resonance. Compared to a classical NFR computation where only ω is a free parameter, there are thus two more unknowns, requiring two additional constraints to have a well-posed problem amenable to continuation, i.e., to describe a one-dimensional manifold to which we refer as THHM locus or simultaneous resonance locus in the sequel. In this work, the first and second constraints prominently affect the frequency and forcing level, respectively. A non-exhaustive list of relevant constraints is detailed hereafter.

(a) Constraint on the frequency

The resonance frequency of a nonlinear system generally depends on the amplitude of vibration. The approach used herein (which was followed in Figure 3b) is to adjust the frequency such that

$$\int_0^{2\pi/\omega} \sin(m\omega t) y(t)\, dt = 0, \tag{3.2}$$

where $y(t)$ represents the response of the structure at some degree of freedom. The one collocated with the forcing (i.e., $y(t) = \mathbf{f}^T\mathbf{x}(t)$) is often considered and is selected in this work. For a primary resonance, this constraint is sometimes referred to as phase resonance, and expresses the fact that the forcing and response are in phase quadrature. It is generally a good approximation of the amplitude peak [40–42]. In this work, we use this as a tracking constraint such that, together with an adequate value for ϕ_l (see Section 3(c)), the two limit cases of the homotopy problem correspond to phase resonances [40], even though the cases in-between may not bear the same interpretation.

Other constraints could be imagined; Equation (3.2) is therefore generally abstracted out as

$$c_1(\mathbf{x}, \omega) = 0. \tag{3.3}$$

(b) Constraint on the forcing

As for the frequency, there exist multiple constraints that one can imagine for the forcing amplitudes, either explicit or implicit. Similarly to Section 2, a first constraint can directly relate the two harmonic forcing amplitudes as

$$\alpha_m f_m + \alpha_l f_l - f = 0, \tag{3.4}$$

where α_m and α_l are user-selected weights for the forcing amplitudes, and f is the maximum weighted harmonic forcing amplitude. When $\alpha_m = \alpha_l$, $f_m|_{f_l=0} = f_l|_{f_m=0}$ and one can thus obtain the different resonances of an NFR (at a given forcing amplitude). This allows for

completing an NFR with its isolated parts, which is one of the main motivating reasons for this constraint, the other one being its simplicity.

Alternatively, motivated by the possibility that the resonance may not change much if it is maintained at a constant amplitude, one may imagine constraining the m^{th} (resonant) harmonic amplitude of its displacement, a_m, to a constant value $a_{m,0}$ as

$$a_m(\mathbf{x}; f_m, f_l) - a_{m,0} = 0, \tag{3.5}$$

making the constraint on f_m and f_l implicit. A more sophisticated constraint is to work with the total (multi-harmonic) displacement amplitude of the resonance a, i.e.,

$$a(\mathbf{x}; f_m, f_l) - a_0 = 0, \tag{3.6}$$

but it is slightly more complex to use given that the amplitude of a Fourier series is not as straightforward to determine [42]. The amplitudes used in this work are those of the response collocated with the forcing ($\mathbf{f}^T\mathbf{x}(t)$), although in principle there is no restriction for the use of non-collocated responses. As shall be shown, using amplitude constraints generally allows for finding a greater number of resonances than the direct forcing constraint (Equation (3.4)), since one has more control on how nonlinear the response is. Because the response amplitude is prescribed, it can also be safer to operate, but has the drawback that the forcing level is no longer explicitly constrained and can become high.

One could imagine other constraints, but the ones given herein appear relevant for the problem at hand. Equations (3.4)-(3.6) can be put under the general constraint form

$$c_2(\mathbf{x}, \omega, f_m, f_l) = 0. \tag{3.7}$$

(c) Selecting the phase shift

For the Duffing oscillator, phase lags at resonance are known analytically [43,44], and this knowledge can be exploited to maximize the chances of success of the THHM. These phase lags are known when the structure is forced with a pure sine: $\phi_r = \pm\pi/2$ when both m and l are odd (the sign depends on the resonance), and $\phi_r = 3\pi/(4l)$ when either m or l is even. To retrieve the sine forcing case, we introduce a time-shifted variable τ such that

$$f_l \sin(l\omega t + \phi_l) = f_l \sin\left(l\omega\left(t + \frac{\phi_l}{l\omega}\right)\right) = f_l \sin(l\omega\tau) \tag{3.8}$$

Let ϕ_r be the known resonant phase lag of the m^{th} harmonic for an m:l resonance. If the structure were forced with that pure sine forcing on the l^{th} harmonic, the m^{th} harmonic of the response at resonance would have a phase lag ϕ_r and could equivalently be expressed as

$$a_m \sin(m\omega\tau - \phi_r) = a_m \sin\left(m\omega\left(t + \frac{\phi_l}{l\omega}\right) - \phi_r\right) = a_m \sin(m\omega t + \phi_m), \tag{3.9}$$

where $\phi_m = -\pi/2$ given that Equation (3.2) holds. Equating the two last terms in Equation (3.9) thus yields a value for the phase shift

$$\phi_l = \frac{l}{m}\left(\phi_r - \frac{\pi}{2}\right) \tag{3.10}$$

which allows for the excitation of the primary and secondary resonances in the limit cases of the homotopy problem, $f_l = 0$ and $f_m = 0$, respectively.

This relation can thus be used to set the phase shift in the THHM problem for the Duffing oscillator. Although these resonant phase lags have been analytically demonstrated for single-degree-of-freedom oscillators, they have been observed to be relevant for multiple-degree-of-freedom systems as well [44,45] and will thus also be heuristically used for the multiple-degree-of-freedom examples treated herein, as they allow for finding relevant resonances. We note however that systems with strong damping nonlinearities may require a more careful treatment [46].

(d) Problem formulation

Equations (3.1), (3.3) and (3.7) are now gathered, yielding

$$\begin{cases} \mathbf{M}\ddot{\mathbf{x}}(t) + \mathbf{C}\dot{\mathbf{x}}(t) + \mathbf{K}\mathbf{x}(t) + \mathbf{f}_{\mathrm{nl}}(\mathbf{x}(t), \dot{\mathbf{x}}(t)) = \mathbf{f}(f_m \sin(m\omega t) + f_l \sin(l\omega t + \phi_l)), \\ c_1(\mathbf{x}, \omega) = 0, \\ c_2(\mathbf{x}, \omega, f_m, f_l) = 0, \end{cases} \tag{3.11}$$

defining a set of point forming the locus followed by the THHM.

Mathematically, the problem described by Equation (3.11) can be solved with a continuation approach to start from a situation where $f_m \neq 0$ and $f_l = 0$ to $f_m = 0$ and $f_l \neq 0$, as described in Section 4. The continuation can also be carried on beyond that point to find other potential intersections of the THHM locus and the $f_m = 0$ plane (as in Figure 3b). With the available knowledge of one of its initial point, the NFR around the target resonance can eventually be computed by setting $f_m = 0$ and fixing the value for f_l found by the THHM.

4. Numerical resolution with the harmonic balance method

A method to compute the solutions of the differential-algebraic equations in Equation (3.11) is now presented. Using a classical HB formalism [19,39], the frequency domain equivalent of Equation (3.11) can be shown to be

$$\begin{cases} \mathbf{A}(\omega)\mathbf{z} + \mathbf{b}_{\mathrm{nl}}(\mathbf{z}, \omega) - \mathbf{b}_m f_m - \mathbf{b}_l(\phi_l) f_l = \mathbf{0}, \\ h_1(\mathbf{z}, \omega) = 0, \\ h_2(\mathbf{z}, \omega, f_m, f_l) = 0, \end{cases} \tag{4.1}$$

where $\mathbf{z}$ is a vector of harmonic coefficients describing a truncated Fourier series for $\mathbf{x}$, i.e.,

$$\mathbf{x}(t) = (\mathbf{Q}(\omega t) \otimes \mathbf{I}_{N_x})\, \mathbf{z}, \tag{4.2}$$

with $\mathbf{I}_n$ is the identity matrix of size n, $\otimes$ denoting the Kronecker product, and

$$\mathbf{Q}(\omega t) = \begin{bmatrix} \frac{1}{\sqrt{2}} & \sin(\omega t) & \cos(\omega t) & \cdots & \sin(N_h \omega t) & \cos(N_h \omega t) \end{bmatrix}. \tag{4.3}$$

If N_h harmonics are used, then the vector $\mathbf{z}$ is of size $N_z = (2N_h + 1)N_x$. The terms appearing in the first line of Equation (4.1) are given by

$$\mathbf{A}(\omega) = \omega^2 \nabla^2 \otimes \mathbf{M} + \omega \nabla \otimes \mathbf{C} + \mathbf{I}_{2N_h+1} \otimes \mathbf{K}, \tag{4.4}$$

with

$$\nabla = \begin{bmatrix} 0 & & & \mathbf{0} \\ & \begin{bmatrix} 1 & 0 & \cdots & 0 \\ 0 & 2 & \cdots & 0 \\ \vdots & \vdots & \ddots & \vdots \\ 0 & 0 & \cdots & N_h \end{bmatrix} \otimes \begin{bmatrix} 0 & -1 \\ 1 & 0 \end{bmatrix} & & \\ \mathbf{0} & & & \end{bmatrix}, \tag{4.5}$$

and $\mathbf{b}_{\mathrm{nl}}(\mathbf{z}, \omega)$ represents the nonlinear forces that can be computed using an alternating frequency-time (AFT) procedure [47]. Furthermore,

$$\mathbf{b}_m = \mathbf{e}_{2m} \otimes \mathbf{f} \tag{4.6}$$

and

$$\mathbf{b}_l(\phi_l) = (\mathbf{e}_{2l} \cos(\phi_l) + \mathbf{e}_{2l+1} \sin(\phi_l)) \otimes \mathbf{f}, \tag{4.7}$$

where $\mathbf{e}_i$ is the i^{th} canonical basis vector of $\mathbb{R}^{2N_h+1}$. Finally, h_1 and h_2 are simply c_1 and c_2 reexpressed with functional dependencies on $\mathbf{z}$ instead of $\mathbf{x}$. These algebraic constraints are detailed in Appendix A(a).

Equation (4.1) defines an algebraic system of equations that maps $\mathbb{R}^{N_z+3}$ to $\mathbb{R}^{N_z+2}$, and is thus solvable with classical continuation tools. A predictor-corrector pseudo-arclength continuation

scheme similar to [19] was used. The strategy to use the THHM in this work goes as follows: the NFR around a primary resonance is first computed with a classical HB continuation. The results are postprocessed to find where phase resonance occurs, giving a starting point for the simultaneous resonance locus. More technical details on the initialization procedure are given in Appendix A(b). The simultaneous resonance locus is computed with a continuation of the solutions of Equation (4.1) until $f_m = 0$.

5. A Duffing oscillator

The Duffing oscillator example introduced in Section 2 is now revisited to show that the proposed method can be used to reach virtually any of its m:l resonances. The THHM is used for isolated ones ($l \neq 1$) since the other ones are attached to the main NFR or bifurcate from it [9]. Once a point on the isola is obtained, the full isola can be computed with a classical continuation approach. The THHM is demonstrated with different constraint choices.

Most of the examples shown herein only disclose the final result of the THHM, namely, the isolated resonance under a harmonic forcing. The responses of the oscillator were computed with $N_h = 31$ harmonics (which allows for the representation of the third harmonic of the resonant motion for all considered m and l in the sequel) and using an AFT procedure with 128 sampling points (which guarantees the absence of aliasing [48]).

(a) Constant-force THHM

The case where the force is kept constant is first investigated; Equation (3.4) (with $\alpha_m = \alpha_l = 1$) is thus used as constraint. A figure in all points identical to Figure 1 is obtained when the THHM is applied to the example considered in Equation (2.1) with $f = 3$ (changing the right-hand side of this equation to adapt it to an m:l resonance according to Equation (3.11)). Considering incommensurate integers m and l between 1 and 9, the method is capable to find multiple isolated resonances, including subharmonic and ultrasubharmonic ones. With this example, the method takes about 21 seconds, including the computation of the main resonance, and the THHM and continuation of a complete isola for every considered resonance. More specifically, the THHM for the 5:3, 3:5, 1:2 and 1:3 resonances takes 1.77 s in total, which favorably compares to the optimistic expected 28 s in Table 1. These results are nevertheless to be taken as rough order-of-magnitude indicators for both approaches given that they are algorithm- and parameter-dependent and that either could further be optimized. We also note that no guesses on the forcing frequency and range of initial conditions are necessary, unlike the stochastic procedure outlined in Section 2(a), but an adequate forcing amplitude is required for both methods.

Figure 5 revisits the example considered in [40] (with $\zeta_0 = 0.005$) with the highest forcing amplitude ($f = 3$). The isolas were found therein through a time-consuming computation of the basins of attraction of the system at different forcing frequencies. As the THHM reveals, there are even more resonances than found before, with 19 different ultrasubharmonic resonances captured by the method. An even larger number of resonances can be found if m and l are allowed to vary beyond 9, but this is not shown herein for brevity and readability reasons. Admittedly, the practical relevance of some of these resonances may be questionable, because of the extreme nonlinear dynamics featured in this example, but also because some of these resonances may have tiny basins of attraction (or not be stable at all) and may thus not be robust against perturbations. Nevertheless, it is interesting to see that the THHM is able to find such a variety of resonances in only about 2 minutes with this example.

(i) Birth of an isolated resonance

The features of the simultaneous resonance curve provide indications as to whether the isola is close to appear in the NFR or not. For illustration, Figure 6 represents the THHM results for the 1:3 resonance (the first isola to appear). For computational simplicity, the process is started from

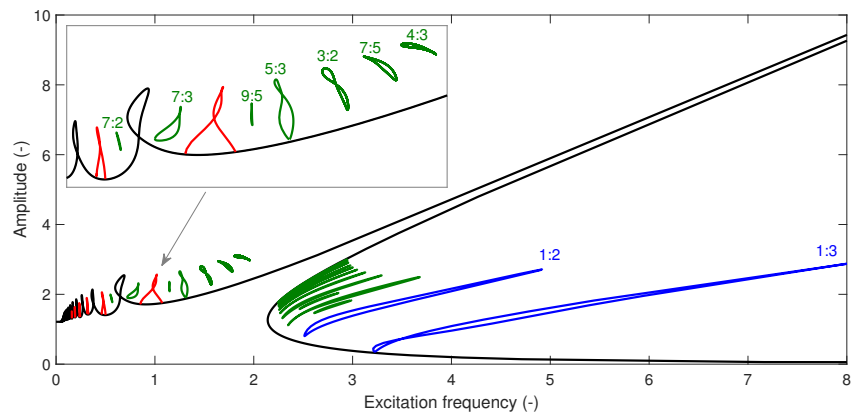

(a)

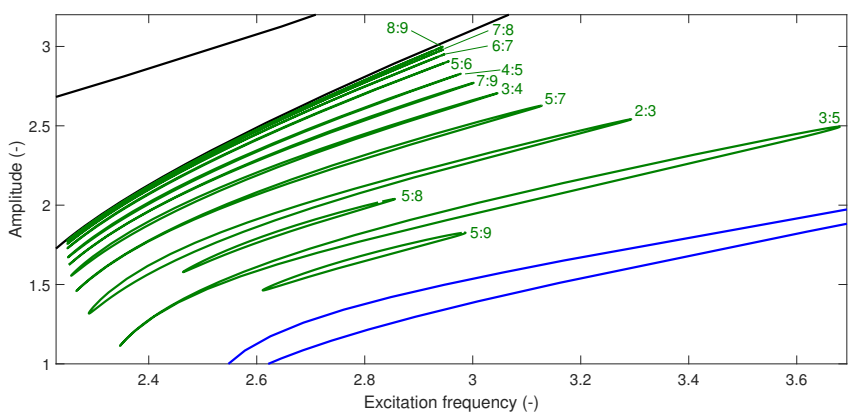

(b)

Figure 5: NFR of the Duffing oscillator $\ddot{x}(t) + 0.01\dot{x}(t) + x(t) + x^3(t) = 3\sin(\omega t)$: main branch of the NFR (—), even superharmonic resonances (—), subharmonic resonances (—) and ultrasubharmonic resonances (—). The NFR is shown in (a), and a close-up on the ultrasubharmonic resonances is shown in (b).

the same 1:1 resonance at $f_m = 1$, but the final f_l is changed by varying α_l, keeping $\alpha_m = 1$ (when $f_m = 0$, $f_l = 1/\alpha_l$ as per Equation (3.4)).

Figure 6a features the THHM loci in the f_m vs. response amplitude plane, starting from $f_m = 1$ and ending when the locus crosses the $f_m = 0$ plane for the last time. In the lowest amplitude case ($f_l|_{f_m=0} = 1$), the THHM locus intersects the $f_m = 0$ plane only at one point corresponding to the absence of subharmonic motion (the method ends up on the main branch of the NFR). At such a low forcing amplitude, the isola does not exist. By contrast, at $f_l|_{f_m=0} = 1.36$, the isola is well developed, and the THHM intersects the $f_m = 0$ plane at three points. One of them is again the main NFR branch, while the two others approximately correspond to the maximum and minimum of the isola. At the intermediate level $f_l|_{f_m=0} = 1.18$, the THHM locus is almost tangent to the $f_m = 0$ plane, and the isola is much less developed. The fold point of the THHM locus considering the forcing amplitude as abscissa is thus of particular interest. Indeed, the quadratic tangency of the simultaneous resonance locus with the $f_m = 0$ plane approximately corresponds

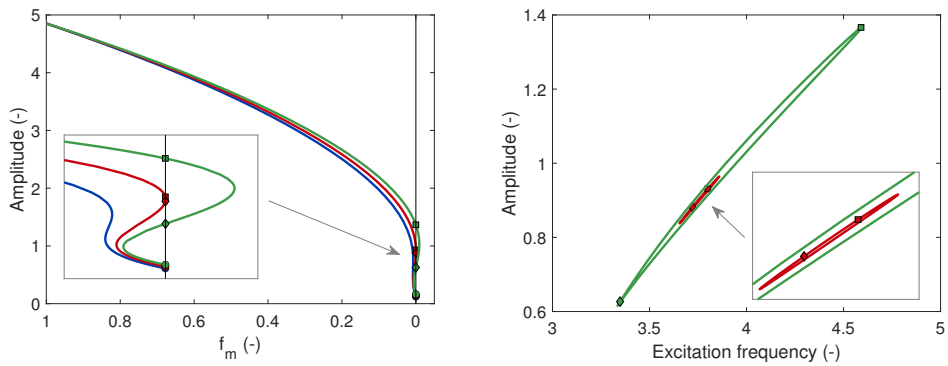

(a) (b)

Figure 6: THHM loci (a) and resulting 1:3 subharmonic resonances (b) starting from $f_m = 1$ with $f_l|_{f_m=0} = 1$ (—), $f_l|_{f_m=0} = 1.18$ (—) and $f_l|_{f_m=0} = 1.36$ (—). The approximate maximum and minimum of the isola, and the main branch of the NFR are indicated by ▫, ◇ and ○, respectively.

to the isola birth. This interesting feature of the THHM can be used to provide a quantitative forcing margin on the appearance of isolas associated to secondary resonances.

(ii) Influence of the phase shift

So far, the phase shift ϕ_l was fixed based on resonance relations. A question then arises: what happens if one selects a different phase shift? Figure 7 provides an answer to this question for the 1:3 resonance (where $\alpha_m = \alpha_l = 1$). Different phase lags ϕ_r were selected, and the phase shifts ϕ_l were computed with Equation (3.10). The THHM loci are shown in Figure 7a. The method essentially fails to find an isolated resonance if the isola associated with the latter does not feature the target phase lag at the specified forcing level, as illustrated by Figure 7b (note that this figure shows the phase *shift*, which is the opposite of the phase *lag* ϕ_r). Specifically, the method is successful and finds a pair of points on the isola for $\phi_r = 5\pi/12$, $\pi/2$ and $7\pi/12$, whereas no subharmonic motion is found when $\phi_r = \pi/3$ or $2\pi/3$, because these phase lags do not exist on the isola at the considered forcing level, as seen in Figure 7b. While this rule is quite simple, it is unfortunately uneasy to know which phase shift to choose in advance for an arbitrary system, but phase lags at resonance are a relevant choice for the Duffing oscillator and can be heuristically used for more complex systems. We also note from Figure 7a that all THHM loci with different phase lags have a common solution, which is associated to an absence of subharmonic motion.

(b) Constant-amplitude THHM

The THHM with constant harmonic amplitude, i.e., where Equation (3.5) is used as constraint, is now considered. For illustration, the method starting from a primary resonance at $f = 0.5$ and considering integers m and l up to 5 is shown in Figure 8. It should be stressed that each one of these resonances is considered at a different final forcing amplitude (gathered in Table 2), and this figure should not be seen as a representation of a single NFR. Figure 8a depicts the harmonic amplitude, showing that the found resonances are peaking at the constrained value of the harmonic amplitude. However, as Figure 8b shows, the resonances have a different shape when the total (multi-harmonic) amplitude of these resonances is plotted. This evidences the importance of the other harmonics in the response and suggests that an approach using the total

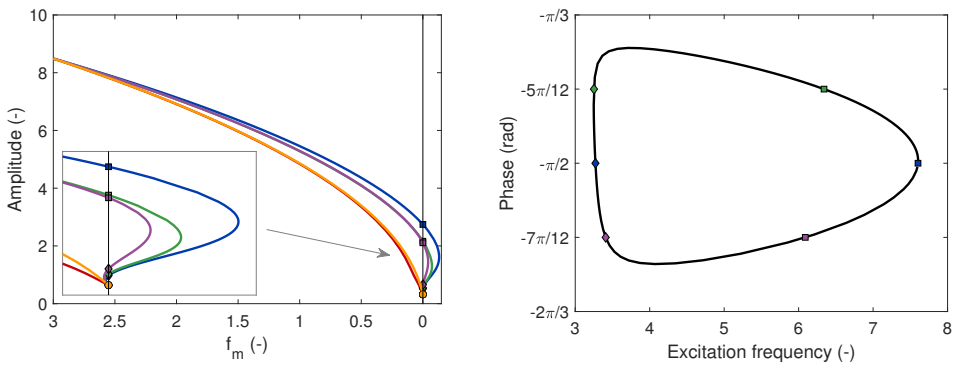

(a) (b)

Figure 7: THHM loci (a) and phase shift of the first harmonic of the 1:3 subharmonic resonance (b) starting from $f_m = 3$ with $\phi_r = \pi/3$ (—), $\phi_r = 5\pi/12$ (—), $\phi_r = \pi/2$ (—), $\phi_r = 7\pi/12$ (—) and $\phi_r = 2\pi/3$ (—). The first, second and thrid (main branch of the NFR) intersection of the loci with the $f_m = 0$ plane are indicated by ▫, ◇ and ○, respectively.

amplitude constraint (Equation (3.6)) would provide different results. In general, the constant-amplitude approach can find a wide variety of resonances; similarly to the case studied in Figure 5, many more resonances can be found if m and l are allowed to go beyond 5.

Resonance	f_l
1:2	23.26
1:3	8.35
1:4	349.75
1:5	136.20
2:3	29.96
2:5	93.47
3:2	40.78
3:4	35.92
4:5	45.25
5:2	136.57

Table 2: Forcing amplitudes required to excite different m:l resonances of the Duffing oscillator $\ddot{x}(t) + 0.05\dot{x}(t) + x(t) + x^3(t) = f_l \sin(\omega t)$ with the constant-amplitude THHM at starting from a primary resonance at $f_m = 0.5$.

6. A two-degree-of-freedom system

A two-degree-of-freedom system characterized by the dimensionless equations

$$\begin{cases} \ddot{x}_1 + 0.01\dot{x}_1 + 0.0144(\dot{x}_1 - \dot{x}_2) + x_1 + 7(x_1 - x_2) + 0.5x_1^3 = f \\ \ddot{x}_2 + 0.01\dot{x}_2 + 0.0144(\dot{x}_2 - \dot{x}_1) + x_2 + 7(x_2 - x_1) = 0 \end{cases} \tag{6.1}$$

is now considered. Its linear resonance frequencies are $\omega_1 = 1$ and $\omega_2 = 3.87$, and the damping ratio on both modes is 0.5%. This system exhibits a 3:1 internal resonance between its two modes, which is responsible for the appearance of an isola in the NFR [42]. With this example, it is shown

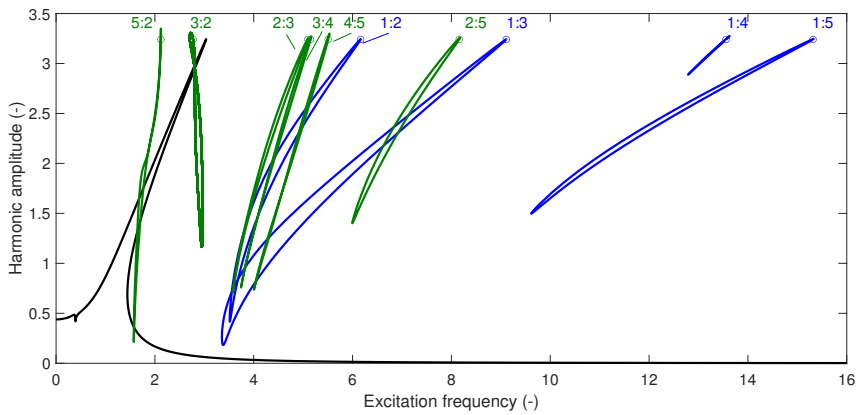

(a)

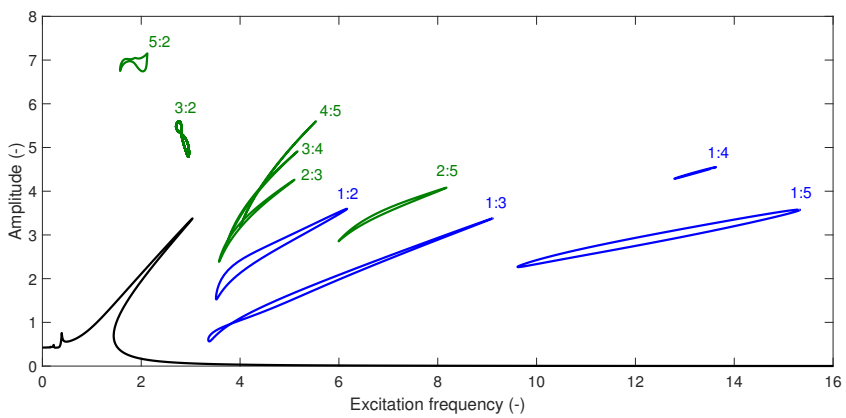

(b)

Figure 8: Harmonic amplitude (a) and total amplitude (b) of the resonances of the Duffing oscillator $\ddot{x}(t) + 0.05\dot{x}(t) + x(t) + x^3(t) = f_l \sin(\omega t)$: primary resonance (—), subharmonic resonances (—) and ultrasubharmonic resonances (—). The initial point found by the constant-amplitude THHM is indicated with ○.

that the THHM effectively finds isolated resonances in multiple-degree-of-freedom systems, and its behavior in the vicinity of an internal resonance is investigated. In what follows, only the response of the first degree of freedom (x_1) is displayed. The same HB parameters and resonant phase lags as in Section 5 were used.

(a) Isolated resonances

The constant-amplitude THHM is used to find several resonances of the two modes. This time, the total amplitude is constrained (i.e., Equation (3.6) is used). The forcing levels on the primary resonances were set empirically to allow for finding multiple isolated resonances.

Figure 9a shows the resonances associated to mode 1 and found by the THHM starting from $f_m = 0.5$. The forcing amplitudes associated with each isola are reported in Table 3a. The THHM has no particular issues finding these isolated resonances. The same test is repeated for mode 2 in Figure 9b with $f_m = 1.5$, which is qualitatively more similar to the Duffing example. The forcing

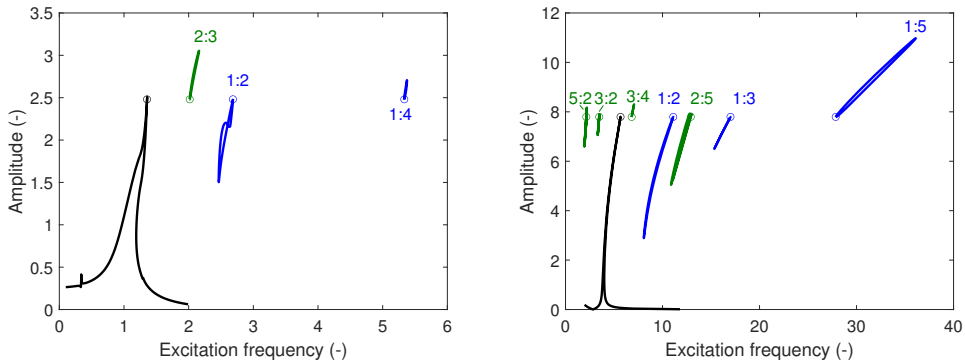

(a) (b)

Figure 9: Total amplitude of the resonances of the two-degree-of-freedom system obtained with the constant-amplitude THHM starting from mode 1 at $f_m = 0.5$ (a) and from mode 2 at $f_m = 1.5$ (b): primary resonance (—), subharmonic resonances (—) and ultrasubharmonic resonances (—). The initial point found by the constant-amplitude THHM is indicated with ∘.

amplitudes are reported in Table 3b. Interestingly, Figure 9 indicates that the THHM sometimes finds points near the local minima of the resonances, which are also characterized by the resonant phase lags [40].

Resonance	f_l
1:2	27.66
1:4	13.34
2:3	8.84

(a)

Resonance	f_l
1:2	62.89
1:3	16.61
1:5	349.55
2:5	24.88
3:2	64.10
3:4	68.68
5:2	18.11

(b)

Table 3: Forcing amplitudes required to excite different m:l resonances of the two-degree-of-freedom system with the constant-amplitude THHM at starting from a primary resonance of mode 1 at $f_m = 0.5$ (a) and a primary resonance of mode 2 at $f_m = 1.5$ (b).

(b) Internal resonances

Forcing levels for which a 3:1 internal resonance between modes 1 and 2 is activated are now considered. This internal resonance can be interpreted as the third harmonic of mode 1 exciting mode 2, or equivalently as the coincidence of the primary resonance of mode 1 and the 3:1 superharmonic resonance of mode 2. Figure 10a features the NFR of the system for a forcing amplitude $f = 0.3$. The isola associated with the internal resonance, found with the constant-force THHM (with $\alpha_m = \alpha_l = 1$) starting from mode 2 and targeting its 3:1 superharmonic resonance, is well developed.

Figure 10a also highlights the points at which the phase resonance condition holds for the third harmonic. The internal resonance results in multiple occurrences of these points in the vicinity of

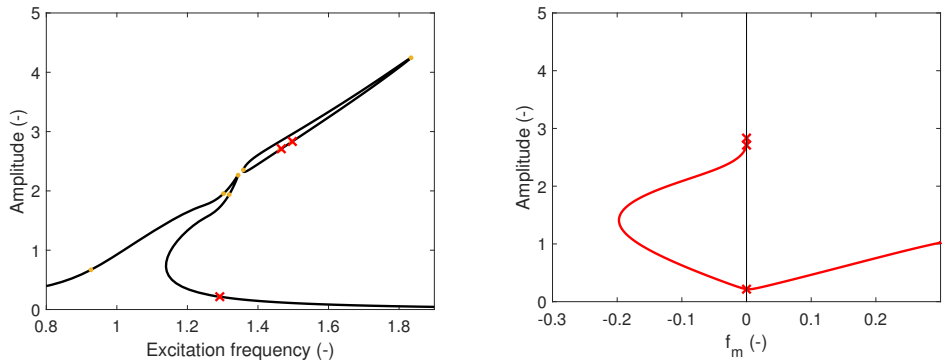

(a) (b)

Figure 10: NFR of the two-degree-of-freedom system under harmonic forcing of amplitude 0.3 (a) and THHM locus for $f_m + f_l = 0.3$ (b). Points where the phase of the third harmonic is equal to $\pm\pi/2$ and intersections of the THHM with the $f_m = 0$ plane are indicated by • and ×, respectively.

the first mode. It can also be seen that the THHM (represented in Figure 10b) captures only a subset of them, but some lie on the isola.

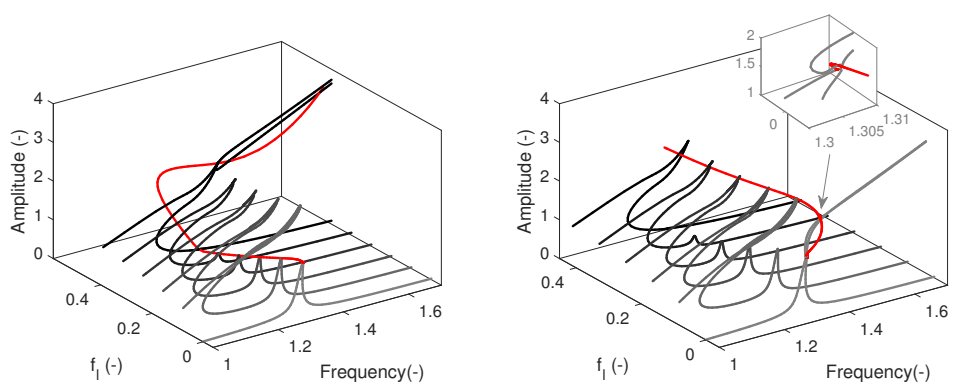

(a) (b)

Figure 11: NFRs of the two-degree-of-freedom system under two-harmonic forcing for $f_m + f_l = 0.39$ (a) and $f_m + f_l = 0.41$ (b). The set NFRs for different values of f_l are given in different levels of gray, and the resonance loci are depicted in red.

Below a forcing amplitude of about 0.4, the constant-force THHM is able to find points on the isola, as shown in Figure 11a. Beyond that amplitude, the method fails to do so (although it still finds a point on the NFR with the correct phase shift) and has a qualitatively different behavior. It can nevertheless be understood if one looks at the NFRs under two-harmonic forcing. In particular, Figure 11b reveal that for $f_m + f_l = 0.41$ the 1:3 subharmonic resonance of the first mode merges with the 1:1 primary resonance of the second mode under a two-harmonic forcing for low values of f_l. The path followed by the THHM is drastically different than when this merging does not occur (cf. Figure 11a, for which $f_m + f_l = 0.39$), and the method is eventually unable to find the isola.

More generally, when an m:l internal resonance occurs, the m:l resonance of one of the internally resonant mode is close to the 1:1 resonance of the second internally resonant mode. Conversely, the l:m resonance of that latter mode is close to the primary resonance of the former mode. A similar scenario can thus be expected to occur for a generic internal resonance, marking a potential limitation of the THHM, and its results should carefully be analyzed. A possible solution could be to generalize the phase resonance criterion with a combination of the phases of multiple harmonics, as has been done in [44,45].

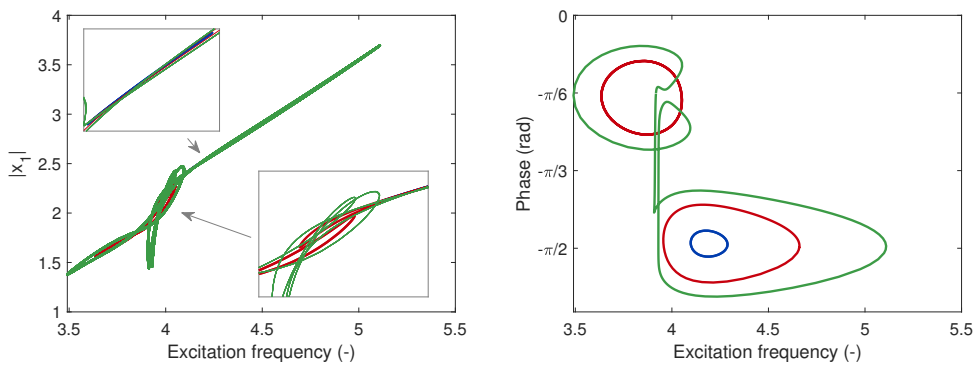

(a) (b)

Figure 12: 1:3 subharmonic resonance of the first mode of the two-degree-of-freedom system at $f_l = 0.22$ (—), $f_l = 0.3$ (—) and $f_l = 0.45$ (—): amplitude (a) and phase of the first harmonic (b).

It is also interesting to investigate more in depth what happens to the 1:3 subharmonic resonance of mode 1 when it is in the vicinity of the primary resonance of mode 2. This isolated resonance is once again found with the constant-force THHM. As Figure 12 reveals, it exists in a rather similar fashion to the Duffing oscillator around $f_l = 0.22$, with a resonant phase lag of $\pi/2$. However, another branch quickly emerges as the forcing grows, with a resonant phase lag of $\pi/6$. This phase lag is equivalent to $-\pi/2$ for this subharmonic regime [40], which is why the THHM finds this isola as well. We note that a two-part 1:3 subharmonic resonance was also evidenced in [49]. The two branches merge around $f_l \approx 0.44$, and beyond that forcing level the isola features a complex topology reminiscent of its two formerly separated constituents. The interplay between internal and secondary resonances thus seems to be an interesting topic of study but is not explored further in this work.

7. A beam with unilateral clearance contact

A more challenging example is now considered, featuring multiple degrees of freedom and an asymmetric, nonsmooth nonlinearity. Since nonsmooth nonlinearities produce a rich spectrum [39], they promote the appearance of secondary resonances [50,51]. This example thus also serves to show that it is possible to observe secondary resonances with realistic vibration amplitudes.

A cantilever beam of dimensions 500 mm $\times$ 20 mm $\times$ 1 mm with a unilateral clearance contact element placed at its tip is considered. The beam is made of steel (Young's modulus $E = 210$ GPa and density $\rho = 7800$ kg/m^3). Figure 13 schematizes the structure. The focus of this study is on the first bending mode and its associated secondary resonances when the tip of the beam is forced and the collocated displacement is monitored.

The beam is modeled with linear Euler-Bernoulli elements including axial, lateral and rotational degrees of freedom. A simple regularized contact law is used and is detailed in

Figure 13: Schematic representation of the beam with clearance contact.

Appendix B. The distance between the neutral fiber of the beam and the contact element is equal to the beam thickness ($x_0 = 1$ mm), and this thickness is neglected when evaluating the nonlinear force (i.e., contact is considered to occur when the neutral fiber clears the gap). The stiffness of the contact k_{nl} was chosen to be 99 times higher than the effective static stiffness at the tip ($3EI/l_x^3$, where I and l_x are the cross-section inertia and beam length, respectively) to mimic a rather hard contact, and the regularization length l_0 was chosen equal to 10 µm. The main numerical parameters, namely the number of elements, harmonics and sampling points for the AFT, were determined based on a convergence analysis, for which only the final conclusions are reported here for brevity. This analysis essentially showed that the results were mostly sensitive to the number of harmonics, and rather insensitive to the number of elements. Accurate computations were achieved above a given number of sampling points allowing to limit the aliasing phenomenon associated with the AFT procedure. As a result, 10 elements, 51 harmonics and 512 sampling points were selected to perform the continuation procedure, offering a reasonable trade-off between accuracy and speed.

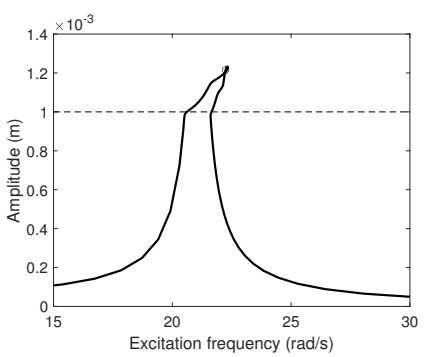

Figure 14: Total amplitude of the beam tip near the primary resonance of its first mode at $f_m = 0.45$ mN (—). A dashed line indicates the amplitude at which contact occurs.

The beam hits the contact at its first resonance when the forcing amplitude reaches 0.0865 mN, and a response at 0.45 mN is considered, i.e., the regime of motion is strongly nonlinear, but features reasonable motion amplitudes. Figure 14 shows the primary resonance of the first mode at this forcing amplitude. The THHM was started from the first mode, and a total amplitude constraint (Equation (3.6)) was used for this example.

As seen in Figure 15, two subharmonic resonances can be found by the THHM at this response amplitude, namely the 1:3 and 1:5 ones at respective forcing levels of 16.2 mN and 20.8 mN. Unsurprisingly, they exist only when the contact force is active, and the tip displacement amplitude is of the order of the thickness of the beam, which is reasonable for a cantilever beam. It should nevertheless be noted that the deflection of the beam under a static load of the same

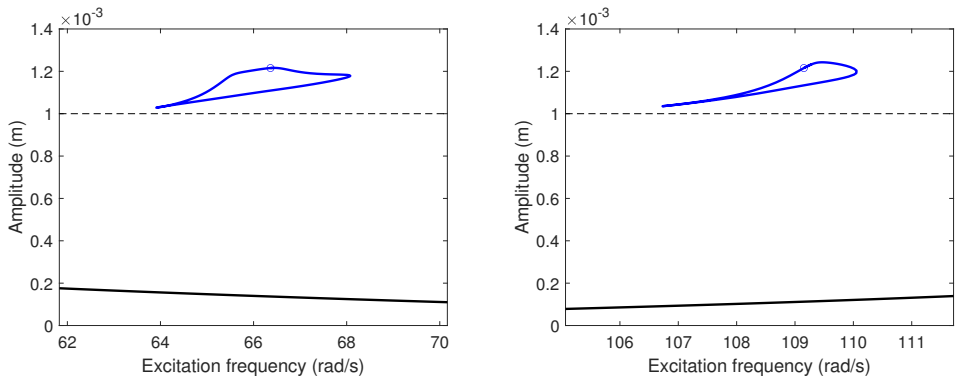

Figure 15: 1:3 subharmonic resonance at $f_l = 16.2$ mN (a) and 1:5 subharmonic resonnace at $f_l = 20.8$ mN (b) of the first mode of the beam (—) and main branch of the NFR at the same forcing level (—). The initial point found by the constant-amplitude THHM is indicated with ○, and a dashed line indicates the amplitude at which contact occurs.

amplitude would lead to the occurrence of contact. The main NFR branches at the same forcing levels as the isolas are also displayed for reference; the isolated resonances feature amplitudes more than 5 times larger.

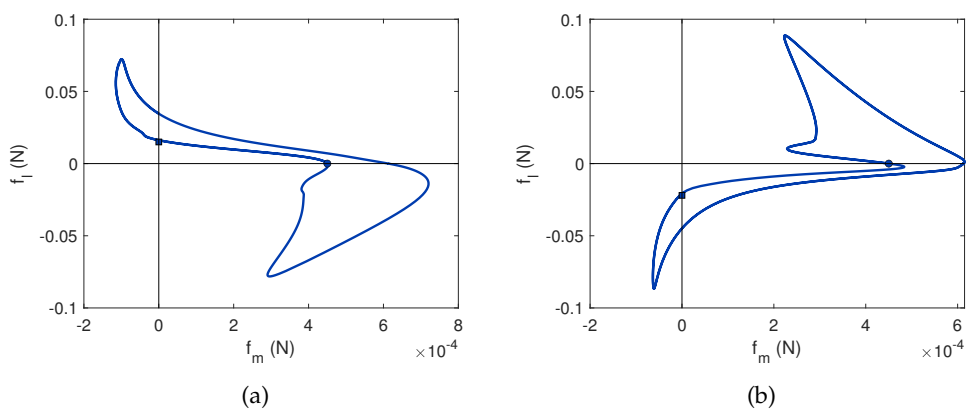

Figure 16: THHM loci for the 1:3 (a) and 1:5 (b) subharmonic resonances of the first mode of the beam. The starting primary resonance is indicated with ○ and the attained subharmonic resonance with ▫.

Figure 16 shows the loci followed by the THHM for the two cases. Since the amplitude is constant, f_l is shown in the ordinate instead. Interestingly, these loci are closed curves that link two primary and two subharmonic resonances together, and no point of the $f_m = 0$ plane corresponds to the main branch of the NFR. Only the resonances associated with the lowest forcing amplitudes are shown herein, because the model may be less reliable for higher forcing amplitudes. It is also interesting to note that the 1:5 resonances occur for a negative value of f_l when a phase lag ϕ_r of $\pi/2$ is selected. By contrast, if a positive forcing amplitude is requested, the resonant phase lag would be -$\pi/2$ (unlike that of $\pi/2$ for the Duffing oscillator). If this phase

lag was selected, Equation (3.10) indicates that $\phi_l = -\pi$ (instead of 0) and Figure 16b would be mirrored about the $f_l = 0$ axis.

The THHM takes 83 s and 113 s for the 1:3 and 1:5 resonances, respectively. A single time integration with a Runge-Kutta solver for stiff problems (`ode15s`) over 500 periods of excitation takes about 3 s (which does not result in a complete disappearance of transients). Estimating the probability based on the basins of attraction (in a similar way to Section 2) in this system with a state-space of dimension 60 would be an impossible task, but one can see that the cost of the THHM is equivalent to a few tens of time integrations, although it should once more be recalled that these quantities are very algorithm- and parameter-dependent.

8. Conclusion

By leveraging two-harmonic forcing, this work proposed a method to connect primary and secondary resonances together. This ad-hoc method relies on the core assumption that this connection exists through states of simultaneous resonances, that can be crossed with a homotopy method. Numerical examples showed that a multitude of isolated resonances can be found rather cheaply without relying on expensive global analysis methods.

The constant-forcing version of the THHM allows to complete the NFR with isolas. The constant-amplitude version of the method generally finds more isolated resonances but has an unpredictable outcome in terms of forcing amplitude. These two versions thus constitute complementary tools. The method fails when there is no homotopy path connecting the starting primary resonance to the sought secondary resonance. This is the case if the secondary resonance does not exist under the constraints selected a priori. Potential limitations were also highlighted in the vicinity of internal resonances. In case of a failure, analyzing the THHM locus may also help the user to gain further insight into the problem at hand.

This work opens the door for several possible extensions. In all examples shown herein, the initial forces were selected empirically to showcase situations where the THHM finds isolated resonances. A predictive capability, i.e., knowing in advance if the method will reach the target resonance, would be an ideal feature, but the strongly nonlinear character of the problems at hand will probably prevent that. Still, the parameter space of THHM is low-dimensional which allows for a fast exploration of this space. This contrasts with the large dimension of the phase space to be explored by global analysis methods. The THHM is quite robust because it builds upon the HB method, which is now very mature. The possibility to track fold bifurcations (with ω as bifurcation parameter) could be interesting to ensure that isolas are followed, since they necessarily possess at least two fold bifurcations. One could also imagine letting ϕ_l free and adding an equation by following the fold bifurcations (with f_l as bifurcation parameter) of the THHM locus to free oneself from the imposition of a preselected phase shift ϕ_l. Finally, the method appears to lend itself to an experimental implementation using control-based vibration testing [38], which will be the subject of future works.

A simplified version of the code used in this work is available at `https://github.com/GhislainRaze/thhm`.

Acknowledgements. Ghislain Raze is a Postdoctoral Researcher of the Fonds de la Recherche Scientifique - FNRS which is gratefully acknowledged.

References

1. Nayfeh AH, Younis MI. 2005 Dynamics of MEMS resonators under superharmonic and subharmonic excitations. *Journal of Micromechanics and Microengineering* **15**, 1840–1847. (10.1088/0960-1317/15/10/008)
2. Heertjes M, van de Wouw N. 2006 Nonlinear dynamics and control of a pneumatic vibration isolator. *Journal of Vibration and Acoustics* **128**, 439–448. (10.1115/1.2128642)
3. Beresnevich VI, Tsyfansky SL. 2005 Characteristic properties of subharmonic oscillations and their application in vibration engineering. *Journal of Sound and Vibration* **280**, 579–593. (10.1016/j.jsv.2003.12.042)

4. Huguet T, Badel A, Druet O, Lallart M. 2018 Drastic bandwidth enhancement of bistable energy harvesters: Study of subharmonic behaviors and their stability robustness. *Applied Energy* **226**, 607–617. (10.1016/j.apenergy.2018.06.011)
5. Anh N, Linh NN, Manh NV, Tuan VA, Kuu NV, Nguyen AT, Elishakoff I. 2020 Efficiency of mono-stable piezoelectric Duffing energy harvester in the secondary resonances by averaging method. Part 1: Sub-harmonic resonance. *International Journal of Non-Linear Mechanics* **126**, 103537. (10.1016/j.ijnonlinmec.2020.103537)
6. Zega V, Silva PB, Geers MGD, Kouznetsova VG. 2020 Experimental proof of emergent subharmonic attenuation zones in a nonlinear locally resonant metamaterial. *Scientific Reports* **10**, 12041. (10.1038/s41598-020-68894-3)
7. Quaegebeur S, Palma ND, Chouvion B, Thouverez F. 2022 Exploiting internal resonances in nonlinear structures with cyclic symmetry as a mean of passive vibration control. *Mechanical Systems and Signal Processing* **178**, 109232. (10.1016/j.ymssp.2022.109232)
8. Parlitz U, Lauterborn W. 1985 Superstructure in the bifurcation set of the Duffing equation. *Physics Letters A* **107**, 351–355. (10.1016/0375-9601(85)90687-5)
9. Marchionne A, Ditlevsen P, Wieczorek S. 2018 Synchronisation vs. resonance: Isolated resonances in damped nonlinear oscillators. *Physica D: Nonlinear Phenomena* **380-381**, 8–16. (10.1016/j.physd.2018.05.004)
10. Sarrouy E, Thouverez F. 2010 Global search of non-linear systems periodic solutions: A rotordynamics application. *Mechanical Systems and Signal Processing* **24**, 1799–1813. (10.1016/j.ymssp.2010.02.001)
11. Sarrouy E, Grolet A, Thouverez F. 2011 Global and bifurcation analysis of a structure with cyclic symmetry. *International Journal of Non-Linear Mechanics* **46**, 727–737. (10.1016/j.ijnonlinmec.2011.02.005)
12. Grolet A, Thouverez F. 2015 Computing multiple periodic solutions of nonlinear vibration problems using the harmonic balance method and Groebner bases. *Mechanical Systems and Signal Processing* **52-53**, 529–547. (10.1016/j.ymssp.2014.07.015)
13. Heinze T, Panning-von Scheidt L, Wallaschek J. 2020 Global detection of detached periodic solution branches of friction-damped mechanical systems. *Nonlinear Dynamics* **99**, 1841–1870. (10.1007/s11071-019-05425-4)
14. Salles L, Staples B, Hoffmann N, Schwingshackl C. 2016 Continuation techniques for analysis of whole aeroengine dynamics with imperfect bifurcations and isolated solutions. *Nonlinear Dynamics* **86**, 1897–1911. (10.1007/s11071-016-3003-y)
15. Ponsioen S, Pedergnana T, Haller G. 2019 Analytic prediction of isolated forced response curves from spectral submanifolds. *Nonlinear Dynamics* **98**, 2755–2773. (10.1007/s11071-019-05023-4)
16. Vadcard T, Thouverez F, Batailly A. 2024 On the detection of nonlinear normal mode-related isolated branches of periodic solutions for high-dimensional nonlinear mechanical systems with frictionless contact interfaces. *Computer Methods in Applied Mechanics and Engineering* **419**, 116641. (10.1016/j.cma.2023.116641)
17. Quaegebeur S, Vadcard T, Thouverez F. 2024 A new numerical path to retrieve isolated branches on large scale nonlinear mechanical systems. *Nonlinear Dynamics*. (10.1007/s11071-024-10369-5)
18. Cenedese M, Haller G. 2020 How do conservative backbone curves perturb into forced responses? A Melnikov function analysis. *Proceedings of the Royal Society A: Mathematical, Physical and Engineering Sciences* **476**, 20190494. (10.1098/rspa.2019.0494)
19. Detroux T, Renson L, Masset L, Kerschen G. 2015 The harmonic balance method for bifurcation analysis of large-scale nonlinear mechanical systems. *Computer Methods in Applied Mechanics and Engineering* **296**, 18–38. (10.1016/j.cma.2015.07.017)
20. Kuether R, Renson L, Detroux T, Grappasonni C, Kerschen G, Allen M. 2015 Nonlinear normal modes, modal interactions and isolated resonance curves. *Journal of Sound and Vibration* **351**, 299–310. (10.1016/j.jsv.2015.04.035)
21. Li M, Jain S, Haller G. 2024 Fast computation and characterization of forced response surfaces via spectral submanifolds and parameter continuation. *Nonlinear Dynamics* **112**, 7771–7797. (10.1007/s11071-024-09482-2)
22. Grenat C, Baguet S, Lamarque CH, Dufour R. 2019 A multi-parametric recursive continuation method for nonlinear dynamical systems. *Mechanical Systems and Signal Processing* **127**, 276–289. (10.1016/j.ymssp.2019.03.011)

23. Mélot A, Goy ED, Renson L. 2024 Control of isolated response curves through optimization of codimension-1 singularities. *Computers & Structures* **299**, 107394. (10.1016/j.compstruc.2024.107394)
24. Friswell MI, Penny JE, Garvey SD, Lees AW. 2000 pp. 113–115. In *Dynamics of Rotating Machinery*, pp. 113–115. CRC Press. (10.1201/9781482270372-11)
25. Claeys M, Sinou JJ, Lambelin JP, Alcoverro B. 2014 Multi-harmonic measurements and numerical simulations of nonlinear vibrations of a beam with non-ideal boundary conditions. *Communications in Nonlinear Science and Numerical Simulation* **19**, 4196–4212. (10.1016/j.cnsns.2014.04.008)
26. Chen Y, Yaghoubi V, Linderholt A, Abrahamsson TJS. 2016 Informative Data for Model Calibration of Locally Nonlinear Structures Based on Multiharmonic Frequency Responses. *Journal of Computational and Nonlinear Dynamics* **11**. (10.1115/1.4033608)
27. Pacini BR, Kuether RJ, Roettgen DR. 2022 Shaker-structure interaction modeling and analysis for nonlinear force appropriation testing. *Mechanical Systems and Signal Processing* **162**, 108000. (10.1016/j.ymssp.2021.108000)
28. Yang J, Qu Z, Hu G. 1996a Duffing equation with two periodic forcings: The phase effect. *Physical Review E* **53**, 4402–4413. (10.1103/PhysRevE.53.4402)
29. Yang HL, Huang ZQ, Ding EJ. 1996b Stabilization of the less stable orbit by a tiny near-resonance periodic signal. *Physical Review E* **54**, R5889–R5892. (10.1103/PhysRevE.54.R5889)
30. Bryant P, Wiesenfeld K. 1986 Suppression of period-doubling and nonlinear parametric effects in periodically perturbed systems. *Physical Review A* **33**, 2525–2543. (10.1103/PhysRevA.33.2525)
31. Vohra ST, Fabiny L, Wiesenfeld K. 1994 Observation of induced subcritical bifurcation by near-resonant perturbations. *Physical Review Letters* **72**, 1333–1336. (10.1103/PhysRevLett.72.1333)
32. Peeters M, Kerschen G, Golinval J. 2011 Dynamic testing of nonlinear vibrating structures using nonlinear normal modes. *Journal of Sound and Vibration* **330**, 486–509. (10.1016/j.jsv.2010.08.028)
33. Nayfeh AH, Mook DT. 1995 *Nonlinear Oscillations*. Wiley. (10.1002/9783527617586)
34. Sato H. 1986 Higher-harmonic Resonance of Duffing-type Nonlinear Systems Excited by a Force Including Higher Harmonics. *Bulletin of JSME* **29**, 2239–2242. (10.1299/jsme1958.29.2239)
35. Fyrillas MM, Szeri AJ. 1998 Control of Ultra- and Subharmonic Resonances. *Journal of Nonlinear Science* **8**, 131–159. (10.1007/s003329900046)
36. Daqaq MF. 2025 On a Class of Periodic Inputs That Passively Quench the Superharmonic Resonance of a Symmetric Duffing Oscillator. *Journal of Computational and Nonlinear Dynamics* **20**. (10.1115/1.4066659)
37. Zhang Y, Zhang Y, Li S. 2017 Combination and simultaneous resonances of gas bubbles oscillating in liquids under dual-frequency acoustic excitation. *Ultrasonics Sonochemistry* **35**, 431–439. (10.1016/j.ultsonch.2016.10.022)
38. Raze G, Abeloos G, Kerschen G. 2024 Experimental continuation in nonlinear dynamics: recent advances and future challenges. *Nonlinear Dynamics* **in press**. (10.1007/s11071-024-10543-9)
39. Krack M, Gross J. 2019 *Harmonic Balance for Nonlinear Vibration Problems*. Mathematical Engineering. Cham: Springer International Publishing. (10.1007/978-3-030-14023-6)
40. Volvert M, Kerschen G. 2021 Phase resonance nonlinear modes of mechanical systems. *Journal of Sound and Vibration* **511**, 116355. (10.1016/j.jsv.2021.116355)
41. Förster A, Krack M. 2016 An efficient method for approximating resonance curves of weakly-damped nonlinear mechanical systems. *Computers & Structures* **169**, 81–90. (10.1016/j.compstruc.2016.03.003)
42. Raze G, Volvert M, Kerschen G. 2024 Tracking amplitude extrema of nonlinear frequency responses using the harmonic balance method. *International Journal for Numerical Methods in Engineering* **125**, 1–28. (10.1002/nme.7376)
43. Volvert M, Kerschen G. 2022 Resonant phase lags of a Duffing oscillator. *International Journal of Non-Linear Mechanics* **146**, 104150. (10.1016/j.ijnonlinmec.2022.104150)
44. Volvert M. 2024 *Resonant phase lags of nonlinear mechanical systems*. PhD thesis University of Liège.
45. Abeloos G. 2022 *Control-based methods for the identification of nonlinear structures*. PhD thesis University of Liège.

46. Porter JH, Brake MR. 2024 Tracking superharmonic resonances for nonlinear vibration of conservative and hysteretic single degree of freedom systems. *Mechanical Systems and Signal Processing* **215**, 111410. (10.1016/j.ymssp.2024.111410)
47. Cameron TM, Griffin JH. 1989 An Alternating Frequency/Time Domain Method for Calculating the Steady-State Response of Nonlinear Dynamic Systems. *Journal of Applied Mechanics* **56**, 149–154. (10.1115/1.3176036)
48. Woiwode L, Balaji NN, Kappauf J, Tubita F, Guillot L, Vergez C, Cochelin B, Grolet A, Krack M. 2020 Comparison of two algorithms for Harmonic Balance and path continuation. *Mechanical Systems and Signal Processing* **136**, 106503. (10.1016/j.ymssp.2019.106503)
49. Yasuda K, Hayashi N. 1982 Subharmonic Oscillations of a Prestressed Circular Plate. *Bulletin of JSME* **25**, 620–630. (10.1299/jsme1958.25.620)
50. Thompson JMT, Bokaian AR, Ghaffari R. 1983 Subharmonic Resonances and Chaotic Motions of a Bilinear Oscillator. *IMA Journal of Applied Mathematics* **31**, 207–234. (10.1093/imamat/31.3.207)
51. Perret-Liaudet J, Rigaud E. 2006 Response of an impacting Hertzian contact to an order-2 subharmonic excitation : Theory and experiments. *Journal of Sound and Vibration* **296**, 319–333. (10.1016/j.jsv.2006.03.004)

A. Details on the harmonic balance implementation

(a) Constraints in the frequency domain

The frequency constraint (Equation (3.2)) is first treated. Using the Fourier series ansatz and the mixed-product property,

$$\begin{aligned}\int_0^{2\pi/\omega} \sin(m\omega t)\mathbf{f}^T\mathbf{x}(t)dt &= \int_0^{2\pi/\omega} \left((\mathbf{Q}(\omega t)\otimes\mathbf{I}_{N_x})(\mathbf{e}_{2m}\otimes\mathbf{f})\right)^T (\mathbf{Q}(\omega t)\otimes\mathbf{I}_{N_x})\mathbf{z}dt \\ &= (\mathbf{e}_{2m}\otimes\mathbf{f})^T \int_0^{2\pi/\omega} (\mathbf{Q}^T(\omega t)\mathbf{Q}(\omega t)\otimes\mathbf{I}_{N_x})dt\mathbf{z}.\end{aligned} \tag{A 1}$$

From the orthogonality of the harmonic functions over one period, it can be shown that the integral is equal to $\pi\mathbf{I}_{N_z}/\omega$. Hence, Equation (3.2) has the frequency-domain counterpart (see also [41])

$$(\mathbf{e}_{2m}\otimes\mathbf{f})^T\mathbf{z} = 0. \tag{A 2}$$

The harmonic amplitude constraint in Equation (3.5) is simply treated by identifying the two relevant harmonic coefficients among $\mathbf{z}$, and taking the 2-norm of the vector formed by these two coefficients. Finally, the total amplitude featured in Equation (3.6) can be computed from $\mathbf{z}$ by casting the Fourier series as a rational polynomial and computing its roots, as explained in [42].

(b) Initialization of the THHM

When initializing the THHM from a 1:1 to an m:l resonance, it should be kept in mind that the period of the sought resonance is m times larger. A reordering of the vector of Fourier coefficients is thus required by multiplying each harmonic index by m. This can be done, e.g., using a harmonic transformation matrix

$$\mathbf{T}_{m:1} = \begin{bmatrix}\mathbf{e}_1 & \mathbf{e}_{2m} & \mathbf{e}_{2m+1} & \cdots & \mathbf{e}_{2hm} & \mathbf{e}_{2hm+1} & \cdots & \mathbf{e}_{2N_hm} & \mathbf{e}_{2N_hm+1}\end{bmatrix}\otimes\mathbf{I}_{N_x}, \tag{A 3}$$

where the number of rows of the first matrix in the Kronecker product can be truncated to $2\tilde{N}_h+1$, where $\tilde{N}_h$ is the number of considered harmonics for the m:l resonance. The start of the simultaneous resonance locus $\mathbf{z}_{1:1}$ can be found from the NFR by monitoring when the phase shift, in this work considered to be

$$\phi = \arctan\left(\frac{(\mathbf{e}_3\otimes\mathbf{f})^T\mathbf{z}}{(\mathbf{e}_2\otimes\mathbf{f})^T\mathbf{z}}\right), \tag{A 4}$$

reaches $-\pi/2$, giving an estimate of the phase resonance $\mathbf{z}_{1:1}$ and its frequency $\omega_{1:1}$. The initial vector of Fourier coefficients for the THHM $\mathbf{z}_{m:l}$ is then

$$\mathbf{z}_{m:l} = \mathbf{T}_{m:1}\mathbf{z}_{1:1}, \tag{A 5}$$

and the frequency $\omega_{m:l}$ is given by

$$\omega_{m:l} = \frac{\omega_{1:1}}{m}. \tag{A 6}$$

B. Regularized clearance contact law

The local displacement in the localized nonlinearity is first computed as

$$x_{\mathrm{nl}} = \mathbf{b}_{\mathrm{nl}}^T\mathbf{x}, \tag{A 1}$$

where $\mathbf{b}_{\mathrm{nl}}$ is an influence vector (typically a Boolean vector whose nonzero entry(ies) correspond to the DoF(s) at which the nonlinearity is located). The clearance contact nonlinear law is then given by

$$\mathbf{f}_{\mathrm{nl}}(x_{\mathrm{nl}}) = \mathbf{b}_{\mathrm{nl}}\frac{k_{\mathrm{nl}}l_0}{2}\left(\log\left(\cosh\left(\frac{x_{\mathrm{nl}}-x_0}{l_0}\right)\right) + \frac{x_{\mathrm{nl}}-x_0}{l_0} + \log(2)\right), \tag{A 2}$$

which can probably more easily be interpreted through its derivative, giving the equivalent stiffness

$$\frac{\partial \mathbf{f}_{\mathrm{nl}}(x_{\mathrm{nl}})}{\partial x_{\mathrm{nl}}} = \frac{k_{\mathrm{nl}}}{2}\left(1+\tanh\left(\frac{x_{\mathrm{nl}}-x_0}{l_0}\right)\right), \tag{A 3}$$

resembling a step function of amplitude k_{nl} and whose transition is localized around $x_{\mathrm{nl}} = x_0$ and occurs over a characteristic length l_0.